THE JOURNAL OF PHYSICAL CHEMISTRY C

Article

Cite This: J. Phys. Chem. C 2019, 123, 5495−5506

pubs.acs.org/JPCC

Deciphering Charge Transfer and Electronic Polarization Effects at Gold Nanocatalysts on Reduced Titania Support

Su-Hyun Yoo,[†] Niklas Siemer,[‡] Mira Todorova,*[,†] Dominik Marx,[‡] and Jörg Neugebauer[†]

[†]Department of Computational Materials Design, Max-Planck-Institut für Eisenforschung GmbH, Max-Planck-Strasse 1, D-40237 Düsseldorf, Germany

[‡]Lehrstuhl für Theoretische Chemie, Ruhr-Universität Bochum, 44780 Bochum, Germany

ABSTRACT: Gold nanoparticles supported on reduced TiO_2 (110) surfaces are widely used as catalysts for oxidation reactions. Despite extensive studies, the role of oxygen vacancies in such systems remains elusive and is controversially discussed. Combining ab initio molecular dynamics simulations with methods originally developed to describe defects in semiconductor physics we study how the electronic charge originally located at the vacancy modifies the charge on the cluster. Despite differences resulting from the employed level of density functional theory (namely semilocal/GGA, GGA + *U*, and hybrid functionals), we consistently find that the Au clusters remain either neutral or acquire a positive charge. The intuitively expected electron transfer from the oxygen vacancy to the gold cluster can be safely ruled out. Analyzing these findings, we discuss the role of the oxygen vacancy in the bonding between Au clusters and support and the catalytic activity of the system.

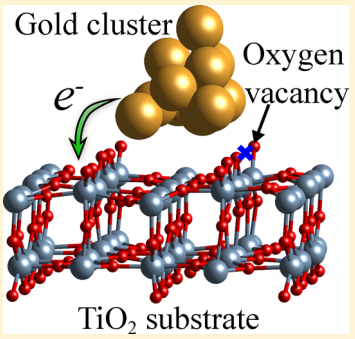

INTRODUCTION

Oxide-supported metal nanoparticles exhibit structural and electronic features which are absent in the individual materials. The resulting properties of the combined system are unique and utilized, for example, to make efficient catalysts.[1−3] In particular, gold nanoclusters supported on reduced titanium dioxide surfaces are a widely studied representative of this class of systems, due to their particular efficiency in catalyzing key chemical reactions, such as the water gas shift reaction,[4,5] the CO oxidation reaction,[2,6−10] and others. Oxygen-deficient TiO_2 surfaces seem to be particularly advantageous in the catalytic context.[11,12] This observation has triggered extensive investigations of reduced, i.e., oxygen-deficient surfaces, which are characterized by a substantial amount of oxygen vacancies. A study combining scanning tunnelling microscopy and density functional theory (DFT) proposed that the vacancy is an active nucleation site for the formation of the Au clusters.[13] Other experimental[14,15] and computational[14,16−19] studies confirmed these findings and revealed that both individual gold atoms and Au clusters preferentially bind to oxygen vacancy sites. There is thus a general consensus that vacancies are important for anchoring gold nanoparticles.

Less clear and controversially discussed are other aspects of the vacancy-cluster interactions. Various DFT studies discuss the character of the bond formed between the Au cluster and the vacancy as being either covalent[13,20] or ionic.[16,21] The type of bonding relates directly to another recent topic - the question whether electronic charge is transferred between gold and the TiO_2 substrate. If present, such a charge transfer could strongly impact the catalytic activity as well as the corresponding chemical reaction mechanisms.[14,21−28] The mechanisms underlying charge transfer are sketched in Figure 1a. The direction of charge transfer is defined by the alignment (relative position) between the defect level of the vacancy and the Fermi level of the nanocluster, in close analogy to the alignment between the redox-levels of molecules. If the defect level is above (below) the Fermi level, the Au cluster will be negatively (positively) charged. Interestingly, there is no agreement in the literature about the direction of the charge transfer, i.e. whether the vacancy donates its electron to the Au cluster,[20,21,23] whether it accepts electrons from it[21] or whether the electrons stay near the vacancy.[13] In general, presence and direction of such a charge transfer are linked to catalytic activity: Having excess electrons/holes at the cluster surface due to negative/positive charging is expected to impact the catalytic behavior of the Au clusters.[20,21,25] In particular, clear indications have been published that small Au nanoclusters pinned at an oxygen vacancy on the TiO_2 (110) surface which are locally positively charged[19,24,26] result in the transfer of hydridic rather than protonic hydrogen to the metal particle in the context of alcohol oxidation reactions.[24,26,28] Clearly, such a transfer of a partially negatively charged hydrogen species to the Au nanocluster would be a high barrier process in the case of a negatively charged nanocluster. Moreover, it has been found that an aqueous phase causes a charge rearrangement at the gold nanocluster producing sites with enhanced positive partial charges by virtue of additional charge transfer between the nanocluster and water,[19] which greatly impacts the liquid-phase heterogeneous catalysis.[28]

Received: December 13, 2018
Revised: January 24, 2019
Published: February 4, 2019

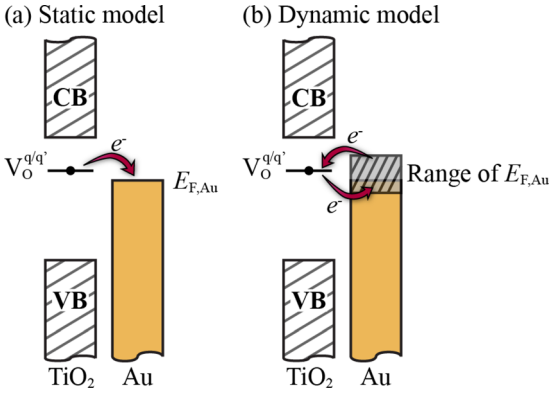

Figure 1. Schematic picture illustrating the differences between the level alignment in a (a) static and (b) dynamic picture. Plotting the relative positions of the Au and TiO_2 energy levels with respect to each other reveals that the gold Fermi energy lies between the valence band (VB) and conduction band (CB) of TiO_2. Charge will be exchanged between the Au Fermi energy and the transition level of the oxygen vacancy ($V_O^{q/q'}$, where q and q' stand for two different charge states of the oxygen vacancy). In the static case (left) the direction of electron transfer is clearly defined (indicated by the red arrow). In the dynamic case (right), charge may be transferred in either direction, i.e., from the Au cluster to the O vacancy or vice versa, as a consequence of the broad distribution of Au Fermi energies due to temperature-induced structural fluctuations of the Au nanocluster.

Most of the previous studies are based on static (T = 0 K) DFT calculations. However, given the small size of the discussed gold clusters (less than 50 atoms) and the temperature at which the catalyst is operative (room temperature and above[4,5,29−38]), temperature-induced structural fluctuations may change the alignment between the defect level and the Fermi level of the cluster with dramatic consequences for the charge transfer. Indeed, previous AIMD studies[19,25] by others and ourselves have already shown that small gold clusters may be rather dynamical objects subject to significant structural fluctuations. While Au clusters deposited at the pristine surface behave similarly to the gas phase, the same clusters pinned by an oxygen vacancy both change structure and become fluxional. Such a dynamic behavior may severely impact the electronic structure (see Figure 1b): A fluctuating gold nanocluster cannot be described by a single value for the Fermi energy. Instead, the Fermi energy broadens and covers a continuous range of values. The consequences for both, charge transfer and bonding, are illustrated in Figure 1b. In contrast to the T = 0 K case (Figure 1a), even the direction of charge transfer may vary in the realistic finite temperature scenario.

As shown in Figure 1, next to temperature-induced broadening, an accurate description of the alignment between defect and Fermi level is critical. It is therefore crucial to assess the underlying electronic structure calculations. Semilocal LDA (local density approximation[39]) and GGA (generalized gradient corrected, e.g., GGA-PBE[40]) calculations, even when applying a +U correction, are known to have deficiencies not only in describing band gaps but also in predicting the position of defect levels and Fermi energies. Errors related to these approximations can get as large as a few electronvolts. Errors of this magnitude can easily override the actual physics and even lead to a spurious charge transfer in the wrong direction.

In the present paper, we therefore most carefully analyze the impact of both, finite temperature effects as well as the impact of the choice of the exchange-correlation (xc) functional. Aiming at providing high-quality references, we compare commonly employed plain GGA-PBE and GGA-PBE + U calculations to hybrid functional ones (namely PBE0[41,42] and HSE06[43,44]). Ab initio molecular dynamics (AIMD) simulations[45] using the GGA-PBE + U approach provide a proper finite-temperature ensemble of fluctuating Au clusters on the reduced rutile surface at the catalytically relevant elevated temperature. To perform the actual electronic structure analysis we make extensive use of concepts originally developed in semiconductor physics. In this community, questions regarding alignment, charge transfer between defects and bands etc. have a long tradition and well-established methodologies exist. For a recent review see for example ref 46.

METHODS

Band Alignment. As discussed in the introduction, band diagrams, like the ones sketched in Figure 1, are a powerful tool to understand whether and how surface defects provide excess charge to a nanocatalyst. Moreover, since they decompose the full system consisting of the nanocatalyst, support and defect into its components, such an approach allows one to study how the thermal fluctuations of the nanoparticle up to the level of shape variations or the choice of the xc-functional affects the electronic structure of each component. Thus, it provides the ideal tool to assess how the choice of the xc-functional or thermal fluctuations affect the magnitude and direction of charge transfer. In the following, we discuss the general steps needed to construct such a band diagram from the DFT calculations.

The full system for which we want to describe the band diagram consists of three major constituents—the gold cluster, the oxygen vacancy, and the TiO_2 substrate. While conceptually the decomposition into the individual parts and the construction of the band diagram are straightforward, performing them with actual DFT codes poses two key challenges: (i) finite-size effects can be present in such calculations due to the limited number of atoms in a DFT supercell and (ii) the lack of an absolute alignment. The lack of an absolute alignment is a direct consequence of periodic DFT calculations: They are invariant against a constant shift in the electrostatic potential. This prevents comparison of the energy levels computed in two separate calculations. As a consequence, the bands shown in Figure 1 for TiO_2 and Au could be shifted against each other by an arbitrary value, making an assessment of charge transfer impossible. We will first focus on the finite-size effects and discuss how they affect the three components (cluster, vacancy, and slab) we consider here.

The TiO_2 support can be formally decomposed into a surface connected to a semi-infinite bulk. In actual DFT calculations, a finite slab consisting of a few atomic layers replaces the semi-infinite bulk. While such finite-size slabs are sufficient to describe surface energy or bonding of adsorbates or clusters with sufficient accuracy, finite-size effects typically cause considerable errors in the electronic structure. For example, for the description of valence and conduction band edges and band gaps unacceptably large errors of a few tenths of an electronvolt are common. The reason is that these states originate for many semiconductors/insulators at the Γ-point.

DOI: 10.1021/acs.jpcc.8b12015
J. Phys. Chem. C 2019, 123, 5495−5506

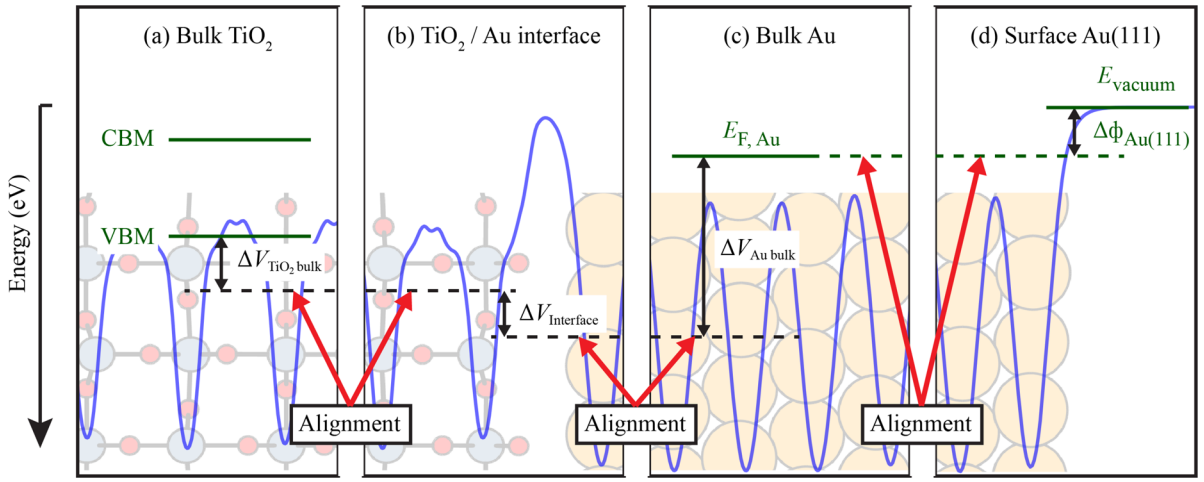

Figure 2. Schematic figure illustrating how band alignment is achieved. The electrostatic potential averaged perpendicular to the displayed direction (in blue) is shown for (a) TiO_2 (bulk), (b) the considered TiO_2/Au interface, (c) Au bulk, and (d) the Au (111) surface. The corresponding atomistic structure is shown in the background. The positions of the TiO_2 (bulk) valence band maximum (VBM) and conduction band minimum (CBM), the Fermi energy of Au (bulk) and the position of the vacuum level used in the surface calculations to determine the Au(111) work function $\Delta\Phi_{Au\ (111)}$, are shown in green. The dashed black lines correspond to the average of the electrostatic potential for the different structures (blue), which is used to obtain the alignment. For details, see text.

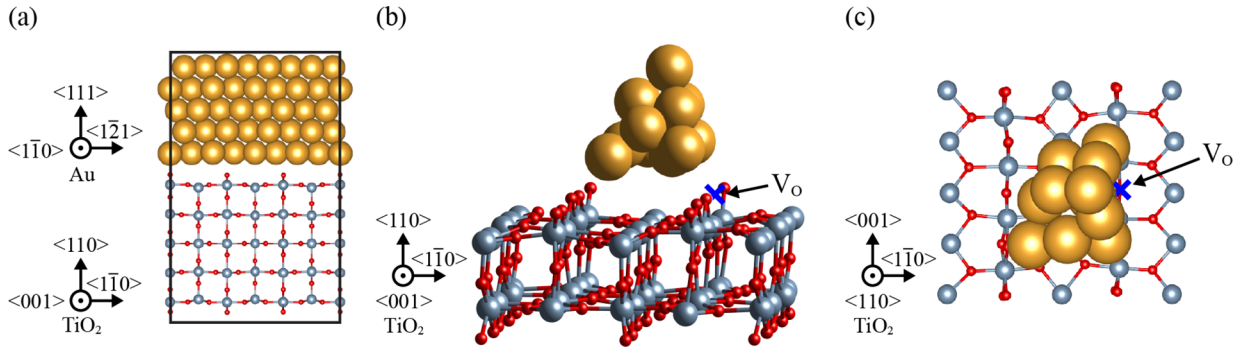

Figure 3. (a) TiO_2 (110)/Au (111) heterostructure used to calculate the band offset between titanium dioxide and gold. (b) Side view and (c) top view of one of the structures of a reduced TiO_2 surface with a Au cluster adsorbed at the oxygen vacancy (V_O) used in the calculations. A blue cross marks the oxygen vacancy. Spheres depict the atoms: oxygen atoms in red, titanium atoms in greyish-blue, and gold atoms in gold.

The long wavelength character of these Bloch states makes them notoriously poor in size convergence.

Following concepts originally developed in semiconductor physics[46] allows one to overcome these convergence issues without requiring larger slab sizes. A key concept in semiconductor band alignment is to utilize the fact that quantities resulting from integration over the entire Brillouin zone, such as the charge density or the electrostatic potential, converge much faster with system size than states related to high symmetry points, such as the Γ-point. Thus, in a first step the average electrostatic bulk potentials $\bar{V}^{\alpha}_{elst}$ which rapidly converge with system size are computed. For the bulk system, it is simply the integral over the unit cell divided by the volume Ω of the cell. For the slab, it is obtained by taking the integral over the bulk-like region in the slab Ω, i.e., in the region a few atomic layers below the surface

$$\bar{V}^{\alpha}_{elst} = \frac{1}{\Omega}\int_{\Omega} V^{\alpha}_{elst}\, d\Omega \tag{1}$$

with α = {bulk or slab}. Since the actual electrostatic average in a perfect bulk or in a bulk-like region far away from the surface has to be the same, knowing the difference between them

$$\Delta V_{elst} = \bar{V}^{bulk}_{elst} - \bar{V}^{slab}_{elst} \tag{2}$$

allows one to align the one-particle energies between slab and bulk calculation

$$\epsilon^{slab}_i = \epsilon^{bulk}_i - \Delta V_{elst} \tag{3}$$

The electrostatic potential differences between bulk and slab are denoted in Figure 2 as $\Delta V_{TiO_2\ bulk}$ and $\Delta V_{Au\ bulk}$, respectively.

The above approach works if the bulk and slab system consist of the same material. To align the band structures of two different bulk materials, the offset between their electrostatic bulk potentials is needed. This offset, $\Delta V_{interface}$, is obtained from an explicit interface calculation and added to eq 3 for one of the materials. The interface calculation is performed employing a heterostructure, i.e. a supercell in which the slab of one material is in direct contact with the slab of the other material, as shown in Figure 3a. The offset between the two bulk electrostatic potentials is calculated as

$$\Delta V_{interface} = \frac{1}{\Omega_I}\int_{\Omega_I} V^{mat_I}_{elst}\, d\Omega_I - \frac{1}{\Omega_{II}}\int_{\Omega_{II}} V^{mat_{II}}_{elst}\, d\Omega_{II} \tag{4}$$

DOI: 10.1021/acs.jpcc.8b12015
J. Phys. Chem. C 2019, 123, 5495−5506

where Ω_I and Ω_{II} are the bulk-like volume parts at each side of the interface over which we perform the integration to obtain the electrostatic potential of the respective material, i.e. $V_{elst}^{mat_I}$ and $V_{elst}^{mat_{II}}$.

Following the procedure outlined above we align the TiO_2 and the Au bulk band structures relative to each other. An essential ingredient to perform this alignment is the possibility to represent the interface between the two materials as epitaxial and to represent it in a moderately sized supercell.

Let us now extend this concept to align the electronic levels of the Au clusters with the TiO_2 support. Because of the small size of the Au clusters consisting of only a few or tens of atoms, finite-size effects in the electronic structure are pronounced. Since these finite-size or quantum confinement effects represent the actual physics we are not allowed to use the alignment obtained for the bulk Au system in order to analyze electronic properties and chemical bonding in case of supported Au nanoparticles. An additional complication arises since at these small cluster sizes Au becomes a semiconductor with a band gap of a few tenth of an electronvolt. Furthermore, even at room temperature atomic vibrations of the Au atoms forming the cluster become large up to the point of inducing shape fluctuations of the metal nanoparticle, which results in non-negligible shifts in the valence and conduction band of the cluster. Thus, an accurate determination of the alignment between a representative ensemble of fluctuating Au clusters and the TiO_2 support at catalytically relevant temperatures is critical.

A possible approach to determine this alignment would be to employ the identical concept used for computing the alignment between bulk Au and TiO_2. Doing this for the actual system, i.e., the Au cluster and the O vacancy at the TiO_2 surface, would result already in a charge transfer. This was not an issue for the bulk alignment, since the (110) TiO_2 surface structure we use is semiconducting, thus providing no donor or acceptor states where electrons can be transferred to or from the Au. To prevent any charge transfer we therefore perform two separate calculations: a calculation for the O vacancy in TiO_2 bulk and another one for the Au cluster. To include the effect the thermal vibrations have on the electronic structure of the small Au clusters we sampled snapshots of Au clusters taken from an actual finite temperature AIMD simulation carried out in the canonical ensemble at T = 450 K as described in the computational details. In these dynamical simulations relying on the GGA-PBE + U approach the Au clusters are placed on a TiO_2 (110) surface with a single O vacancy as depicted in parts b and c of Figure 3 for one representative snapshot configuration. Note that an Au cluster adsorbed at the pristine surface has been shown previously to move rather freely and to even conserve its gas phase structure after deposition, while the same cluster essentially melts if it gets anchored at an oxygen vacancy.[25] Moreover, there is experimental evidence that these clusters get pinned at oxygen vacancies on titania surfaces, whereas they start to sinter once all such vacancies are occupied.[15] Therefore, we restrict our investigation to the catalytically relevant scenario where the Au cluster is pinned at such a vacancy, thus being subject to considerable thermal fluctuations.

The central step in the alignment shown in Figure 2 requires bringing the two separate systems together. Unfortunately, performing a joint calculation of the cluster on the surface with vacancy could result in charge transfer. Since such a charge transfer would affect the alignment we employ another well-established concept from semiconductor theory—absolute alignment. The key idea is to reference both calculations to the same reference, commonly the vacuum level. Translated to our problem, this means that we compute in a first step the alignment of the TiO_2 valence and conduction band to the vacuum level.

In practical DFT supercell calculations, the work function, which can be regarded as the Fermi level referenced to the vacuum potential, is conceptually easier to compute for a metal than for a semiconductor. The reason is the very efficient electronic screening (and the ensuing negligible self-interaction error) and the fact that the work function does not depend on doping. We thus align the bulk bands of TiO_2 to the vacuum level via a series of three individual alignments shown in Figure 2.

For the Au cluster, we can carry out the alignment with respect to the vacuum level directly, i.e., by determining the difference between the Fermi level and the constant electrostatic potential in the vacuum, i.e., far away from the Au cluster. Having for both the bands of TiO_2 bulk and the Au clusters the alignment with respect to the same level—the vacuum potential—allows us to reference these levels *before* charge transfer.

The remaining task is to determine the position of the defect states of the O vacancy on an absolute scale. As mentioned above, well-established approaches exist to perform these calculations. For a detailed discussion, see, e.g., refs 46 and 53. In the following, we will use defect levels obtained from calculations for an oxygen vacancy in bulk TiO_2, as they present a reasonable first approximation to the defect levels of an oxygen vacancy at the TiO_2 surface. Only most recently has a scheme correcting the spurious interactions arising between periodically repeated charged point defects at a surface or interface become available.[54] Therefore, if needed, defect levels for an oxygen vacancy at the TiO_2 surface can now be computed accurately, as well. The procedure to do so remains the same, but the TiO_2 bulk in the required supercell calculations with and without a defect has to be replaced by a slab.

Computational Details. All static density-functional theory (DFT) calculations are performed using the Vienna *ab initio* simulations package (VASP) .[55−59] The employed projector augmented wave (PAW) method[60] was used with a kinetic-energy cutoff of 500 eV for the plane-wave basis set. A total of 6, 12, and 11 electrons are treated as valence states for O, Ti, and Au, respectively. Γ-centered k-point grids with (4 × 4 × 6) k-points for rutile TiO_2 and (8 × 8 × 6) k-points for fcc Au bulk are used for Brillouin-zone integrations. Equivalently folded meshes are used for all other structures. The atomic geometry and electronic structures are calculated using the generalized gradient approximation (GGA) by Perdew, Burke, and Ernzerhof (PBE),[40,61] a Hubbard U augmented method (PBE + U) in which a self-consistently computed linear-response theory based[62,63] U-parameter of U = 4.2 eV[64] is applied to the Ti 3d states,[65] and the hybrid functionals PBE0[41,42] and HSE06[43,44] in which an amount α of Hartree−Fock (HF) exchange is intermixed with the PBE exchange. For the hybrid functionals (PBE0 and HSE06), where the Coulomb potential for exchange is partitioned into a short-range and a long-range part, the recommended[66] screening parameter of ω = 0.11 $bohr^{-1}$ is consistently used. Since the hybrid functionals overestimate the band gap energy of TiO_2 when the default HF-mixing of α = 0.25 is used, we also

DOI: 10.1021/acs.jpcc.8b12015
J. Phys. Chem. C 2019, 123, 5495−5506

Table 1. Calculated Bulk Properties for Rutile TiO_2: Equilibrium Lattice Constant a, c/a Ratio, Direct Band Gap Energy E_g, and Heat of Formation ΔH_f[a]

xc-functional	a_0 (Å)	c/a	E_g (eV)	ΔH_f (eV/f.u.)
PBE	4.652 (1.3)	0.639 (−1.0)	1.803 (−40.5)	−9.06 (−7.4)
PBE + U (U = 4.2 eV)	4.673 (1.8)	0.648 (0.3)	2.244 (−25.9)	−9.42 (−3.6)
PBE0 (α = 0.15)	4.610 (0.4)	0.642 (−0.4)	3.162 (4.4)	−9.39 (−4.0)
PBE0 (α = 0.25)	4.588 (−0.1)	0.644 (−0.2)	4.138 (36.6)	−9.64 (−1.5)
HSE06 (α = 0.20)	4.601 (0.2)	0.643 (−0.4)	3.033 (0.1)	−9.48 (−3.0)
HSE06 (α = 0.25)	4.589 (0.0)	0.644 (−0.2)	3.370 (11.2)	−9.60 (−1.8)
PBE[47]	4.65	0.639	1.77	−9.33
HSE06[47] (α = 0.20)	4.59	0.642	3.05	−9.73
experiment	4.594[48,49]	0.645[48,49]	3.03[50,51]	−9.78[49]

[a]Deviations from the respective experimental values (in percent) are shown in brackets. Literature values are reported in the last three rows and are taken from the cited publications.

performed calculations using mixing values reproducing the experimental band gap, i.e., α = 15% for PBE0 and α = 20% for HSE06. The modified α values are determined following the approach of ref 47.

For the slab calculations of rutile TiO_2(110) an asymmetric slab with four O−Ti−O triple layers and 13 Å of vacuum is constructed for a $p(4 \times 2)$ surface unit cell. Partially filled O and Ti dangling bonds at the $TiO_2(\bar{1}10)$ surface are passivated by pseudohydrogen atoms of valence 2/3 e^- for the O dangling bonds and 4/3 e^- for the Ti dangling bonds, to mimic a bulk-like system; this specific slab model has been introduced and carefully benchmarked in extensive convergence tests in ref 67.

In order to investigate the charge states of the oxygen vacancy V_O we used a $(2 \times 2 \times 3)$ rutile TiO_2 supercell from which a single oxygen atom is removed. To check the convergence and exclude the influence of spurious interactions between periodic images of the changed oxygen defect we also considered in addition a $(3 \times 3 \times 4)$, a $(3 \times 3 \times 5)$ and a $(4 \times 4 \times 6)$ supercells. Because experimental observations[68−70] and the hydrogenic model[71] indicate that the V_O in TiO_2 is a shallow donor defect, the shallow donor correction introduced in ref 46 is applied in each case. We find that the results obtained for the $(2 \times 2 \times 3)$ supercell are consistent with the results for the bigger cells. The calculations were performed for each possible defect state with each of the mentioned exchange-correlation functionals employing the respective equilibrium lattice parameters for bulk rutile TiO_2.

The investgated Au nanoclusters contain 11 atoms and are located at the vacancy site on the TiO_2 (110) surface as described above. The alignment within the Au-cluster/reduced TiO_2 (110) system has been studied based on 20 uncorrelated configuration snapshots as follows. In order to rigorously generate thermal fluctuation effects, AIMD simulations[45] of that system[19] have been carried out in the canonical ensemble at a catalytically relevant temperature of 450 K. The trajectory has been generated using the PBE + U implementation[63] in the Car−Parrinello molecular dynamics (CPMD) program package[72] using the aforementioned U = 4.2 eV.[64] After some equilibration period, we sampled 20 snapshots each 360 fs.

RESULTS

Band Diagram for the Au Cluster/Reduced TiO_2 (110) System. We now describe the actual calculations used to perform the alignment described in the previous section. As discussed and schematically sketched in Figure 2, we first determine the alignment between bulk TiO_2 and Au on an absolute scale. To perform the necessary calculations we use several different supercells. We construct the heterostructure using a five-layer Au (111) slab and a five O−Ti−O trilayer TiO_2 (110) slab. The resulting Au(111)/TiO_2(110) interface is shown in Figure 3a. The lateral dimensions of the interface unit cell are defined by the support, i.e., the TiO_2 lattice parameters. Because of the lattice mismatch between the TiO_2 and Au lattices the Au slab is laterally stained. On the basis of the computationally determined equilibrium lattice constants we find a lattice mismatch in the range of 3.0% to 4.4% between TiO_2 $\langle 1\bar{1}0 \rangle$ and Au $\langle 1\bar{2}1 \rangle$ and of −0.5% to −2.5% between TiO_2 $\langle 001 \rangle$ and Au $\langle \bar{1}10 \rangle$, depending on the choice of functional. The lattice mismatch values obtained for PBE + U (3% for TiO_2 $\langle 1\bar{1}0 \rangle$//Au $\langle 1\bar{2}1 \rangle$ and −2.5% for TiO_2 $\langle 001 \rangle$// Au $\langle \bar{1}10 \rangle$) are closest to the experimental ones of 2.1% and −2.9%, respectively. The U value used here and throughout the manuscript has been computed self-consistently from linear response theory[62−64] and has not been adjusted any further to match experimental observables.

To determine the work function of Au we use a supercell containing a 13-layer Au (111) slab and a 18 Å vacuum region. To perform the absolute alignment for the Au clusters we use 20 uncorrelated snapshots of nanocluster configurations consisting of 11 Au atoms on a reduced TiO_2 (110) support sampled from an AIMD trajectory as explained in the computational details. Recall that Au clusters on the pristine surface neither show pronounced thermal fluctuations[25] nor are catalytically relevant due to sintering[15] and, therefore, are not considered here. We estimate the performance of the various DFT xc approximations by performing calculations using several different xc-functionals. The plain GGA-PBE[40] xc-functional is standardly used in DFT calculations. Unfortunately, it underestimates the band gap of TiO_2 by almost 40%, as can be seen from calculations by others and by us (Table 1). An alternative to GGA-PBE, which improves the description of the TiO_2 band gap at a similar computational cost, is the augmentation of this functional by an U-parameter[65] applied to the Ti 3d states. The value of U = 4.2 eV used within this work has been computed[64] from the self-consistent linear-response technique[62,63] without any adjustment. The resulting GGA-PBE + U method has been extensively used in AIMD simulations of excess electron dynamics at the reduced TiO_2 (110) surface,[64] and to study properties and catalytic reactions using the Au/TiO_2 system.[18,19,24,26] Applying the self-consistently determined Hubbard correction U reduces the error in the band gap and the formation energy by half, at similar accuracy for the lattice parameters.

DOI: 10.1021/acs.jpcc.8b12015
J. Phys. Chem. C 2019, 123, 5495−5506

The two hybrid functionals PBE0[41,42] and HSE06[43,44] with standard mixing (α = 0.25) improve the description of the lattice parameters and the formation energy, but overshoot when it comes to the description of the band gap. In the case of PBE0 the band gap error is almost as large as the plain PBE one, albeit in the opposite direction. Reducing the amount of exact exchange in PBE0 to α = 0.15 and in HSE06 to α = 0.20[47] significantly improves the description of the band gap, while retaining a similar accuracy for the remaining materials properties, as can be seen in Table 1.

The Au(111) work function and the band offset between Au and TiO_2 calculated using the Au/TiO_2 heterostructure shown in Figure 3a are also listed in Table 2. Here, a positive value for the band offset indicates that the valence band of TiO_2 lies below the Au Fermi energy, i.e. further away from the vacuum level. Note that, because the on-site potential U is only applied to the Ti 3d states, the PBE work function of Au(111) is used for the absolute alignment in the PBE + U case.

Table 2. Work Function $\Delta\Phi$ Calculated for the Au (111) Surface and Band Offset ΔV Obtained from a Calculation for a Au/TiO_2 Heterostructure

xc-functional	$\Delta\Phi$ (eV)	ΔV (eV)
PBE	5.19	−0.42
PBE + U (U = 4.2 eV)		0.38
PBE0 (α = 0.15)	5.18	0.13
PBE0 (α = 0.25)	5.17	0.54
HSE06 (α = 0.20)	5.13	0.19
HSE06 (α = 0.25)	5.12	0.42
experiment	5.1 ± 0.1[52]	

The energy levels calculated for TiO_2 with different functionals are listed in Table 3. We can compare these values, because we aligned the calculated energies on an absolute scale. A comparison of the VBM and CBM positions obtained with the different functionals reveals that PBE + U and the hybrid functionals improve the PBE band structure description by down-shifting the VBM position. In comparison, shifts in the CBM values or the positions of the transition states are much smaller.

Using the listed values we construct for the reduced TiO_2/Au cluster system a band diagram for each employed xc-functional. Before we discuss these results, let us first consider the band diagram constructed from the HSE06 calculations shown Figure 4a. The left-most band structure is for TiO_2 and shows next to its band edges the regions within the TiO_2 band gap where the oxygen vacancy is stable in a given charge state. Here, the vacancy V_O in the +2 charge state (green region) is stable over the predominant part of the band gap, while the +1 charge state (orange region) becomes stable in the vicinity of the conduction band minimum (CBM). The boundary line between the two colored regions gives the transition level between these two charge states. The remaining four band diagrams in Figure 4a relate to the Au clusters. Because of thermal fluctuations, the various Au clusters are structurally different. As a consequence, each of them has its own distinct VBM, CBM, and band gap. Three selected clusters shown in the right part of Figure 4a illustrate these effects. These are the initial cluster (sampled from the initial part of the AIMD simulation) shown in Figure 3a, the cluster with the highest and the cluster with the lowest VBM. We thus obtain the temperature induced spread in the VBM and CBM. To account for temperature induced broadening of the bands, which may lead to a disappearance of the band gap at elevated temperatures, we also show the E_F positions of the Au clusters as the middle of the band gap. This spread is highlighted in the Au band diagram shown next to the TiO_2 band structure by the red and the blue shaded regions. The actual values defining this distribution are compiled in the histogram on the right and are enlarged in Figure 4b. The spread with respect to the used functionals is shown in Figure 4c.

Origin and Direction of Charge Transfer. The constructed band diagram for the reduced TiO_2/Au-cluster system enables us to discuss the direction of charge transfer in the system. For an oxygen vacancy to assume a given charge state the corresponding number of electrons must be transferred to or from the gold cluster. For example, a doubly positively charged oxygen vacancy V_O^{2+} can be realized if two electrons from the vacancy are transferred to the CBM of the gold cluster. Such a transfer can occur only if the CBM is lower in energy than the respective charge transition level of the defect. For the discussed example this means that there must be a CBM value which lies below the transition level given by the boundary between the green and the orange regions in the TiO_2 band gap. Since the lowest CBM value we calculated for the Au clusters aligns with the CBM of TiO_2, a V_O^{2+} defect cannot be realized by a charge transfer to the gold cluster. However, the VBM positions of several Au clusters lie higher in energy than the CBM of TiO_2. For these, a transfer of electrons from the Au to the TiO_2 is expected to occur, which will result in a positive charge on the Au cluster solely as a result of thermal fluctuation effects of the supported metal nanoparticle.

We find a spread in the VBM and CBM values calculated for the gold clusters with the various xc-functionals we use, as seen in the band diagrams shown in Figure 5. The covered energy range is rather different. Both PBE and PBE + U suggest a rather narrow spread of energies for both the VBM and CBM, while the hybrid functionals extend over a much wider range of energies. The much larger spread of valence and conduction

Table 3. Position of the Valence Band Maximum (VBM) and Conduction Band Minimum (CBM) of TiO_2 and of the Transition Level of an Oxygen Vacancy V_O^q in TiO_2 Bulk on an Absolute Scale, i.e., with Respect to the Vacuum Level, in Electronvolts

xc-functional	VBM	CBM	+1/0	+2/0	+2/ + 1
PBE	−6.58	−4.78	−4.80	−4.85	−4.91
PBE + U (U = 4.2 eV)	−7.24	−5.00	−5.37	−5.26	−5.15
PBE0 (α = 0.15)	−7.62	−4.46	−4.32	−4.55	−4.78
PBE0 (α = 0.25)	−8.40	−4.26	−4.83	−4.79	−4.76
HSE06 (α = 0.20)	−7.52	−4.49	−4.31	−4.50	−4.69
HSE06 (α = 0.25)	−7.87	−4.50	−4.57	−4.53	−4.48

DOI: 10.1021/acs.jpcc.8b12015
J. Phys. Chem. C 2019, 123, 5495−5506

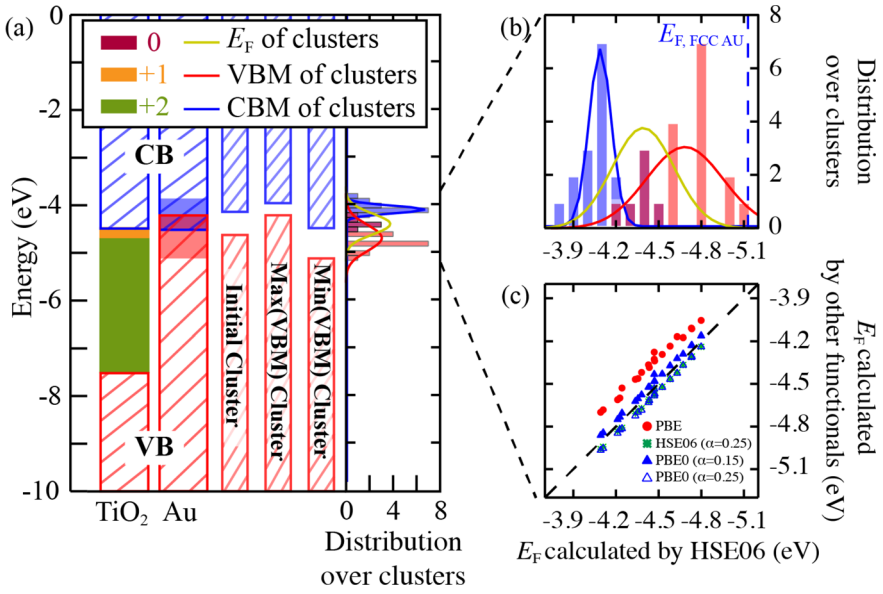

Figure 4. (a) Band alignment for the Au/V_O:TiO_2 system on an absolute scale obtained by HSE06 (α = 0.20) calculations. The valence band (VB) is shown in red and the conduction band (CB) in blue. The red shaded area at the top of the VB of Au and the blue shaded area at the bottom of the CB of Au show the range of the VB maxima and CB minima obtained for different gold clusters. Shown are also the band structures of three representative Au clusters (see text). The distribution of VB maxima (red) and CB minima (blue) for all the considered Au clusters from uncorrelated snapshots of the AIMD trajectory is shown in the left part of the figure. The middle of each band gap is used to plot the distribution denoted by E_F (yellow). (b) Zoom-in into the band edges distribution of the clusters. (c) Plot showing the correlation between the Fermi energy (see above) of the gold clusters calculated by HSE06 (α = 0.20) in comparison to the other used exchange-correlation functionals. Since the on-site potential U is only applied to the Ti 3d states and we use calculations involving solely the gold nanoparticles for their alignment on the absolute scale (see text), the PBE and the PBE + U results are identical.

band in all calculations using hybrid functionals may be not a purely electronic effect but could also indicate that the energy of the clusters is very different. If this would be the case the snapshots obtained from AIMD simulations using PBE + U may not be applicable to hybrid functionals. To test the impact of the functional we computed for each of the cluster configurations and for each xc-functional the cluster energy per atom referenced to the atom energy in Au bulk. The results are shown for each functional in the right-most histogram with purple bars. As can be seen, the width due to thermal broadening is very similar for all functionals, indicating that the large differences in the electronic structure found by the various functionals have only a small impact on the energetics and thus the trajectories. This insight allows us to use in the following for each functional the same set of cluster structures as obtained from AIMD using the PBE + U functional. Figure 5 further shows that the Fermi energy of the clusters is systematically higher than the one for the Au bulk. This behavior is a direct consequence of the pronounced spatial quantum confinement of the electrons in the Au clusters.

In the following, we use the results collected in Figure 5 to discuss the impact the xc-functional has on the direction and magnitude of the charge transfer between the cluster and the vacancy. Let us start with the limiting case where the Au cluster is replaced by Au bulk. In this case, finite-size effects, as well as thermal fluctuations, can be neglected. As shown by the black dashed line in Figure 5, a very consistent result is found: The charge state of the vacancy is in all cases, except for a single xc-functional (PBE+U), +2. This implies that the vacancy transfers two electrons to the Au, which would become as a consequence negatively charged. The only exception is found for the PBE + U calculation where the vacancy remains uncharged, i.e. no electron transfer occurs.

Let us now discuss the impact of spatial localization and thermal fluctuations on this picture. As mentioned before, for the small cluster sizes even Au, which is metallic in its bulk phase, opens a sizable band gap of a few tenths of an electronvolt. A charge transfer can thus be only realized if the bottom of the Au cluster conduction band drops below the energy level where the vacancy becomes positively charged, i.e., where it can donate its electrons. Note that also an electron charge transfer from the Au to the TiO_2 surface (not the vacancy) becomes possible, if the Au valence band moves above the TiO_2 conduction band.

As can be seen from the data shown in Figure 5 the CBM of the Au clusters is practically always above the CBM of TiO_2, i.e. there will be no charge transfer from the vacancy to the Au clusters. This finding applies to all cluster configurations and is, very importantly, independent of the choice of xc-functional. This is an unexpected result in view of the large variation in the electronic structure with respect to band gaps of the Au and the spread due to thermal excitations.

Let us now consider the second possible mechanism of charge transfer, i.e., the one that is not related to the vacancy. This mechanism is thus not specific, but it would occur even if the cluster was not attached to a surface vacancy. As shown in Figure 5 for the semilocal xc-functionals, this mechanism will be active for essentially all cluster configurations, whereas for the hybrid functionals it is only active for some cluster configurations, while others show no charge transfer. For this mechanism, the choice of the xc-functional affects the result qualitatively. The semilocal xc-functionals predict a full charge transfer whereas for the hybrid functionals the charge transfer fluctuates strongly. This mechanism can thus provide (positive) excess charge on the clusters and consequently make them catalytically more active.

DOI: 10.1021/acs.jpcc.8b12015
J. Phys. Chem. C 2019, 123, 5495−5506

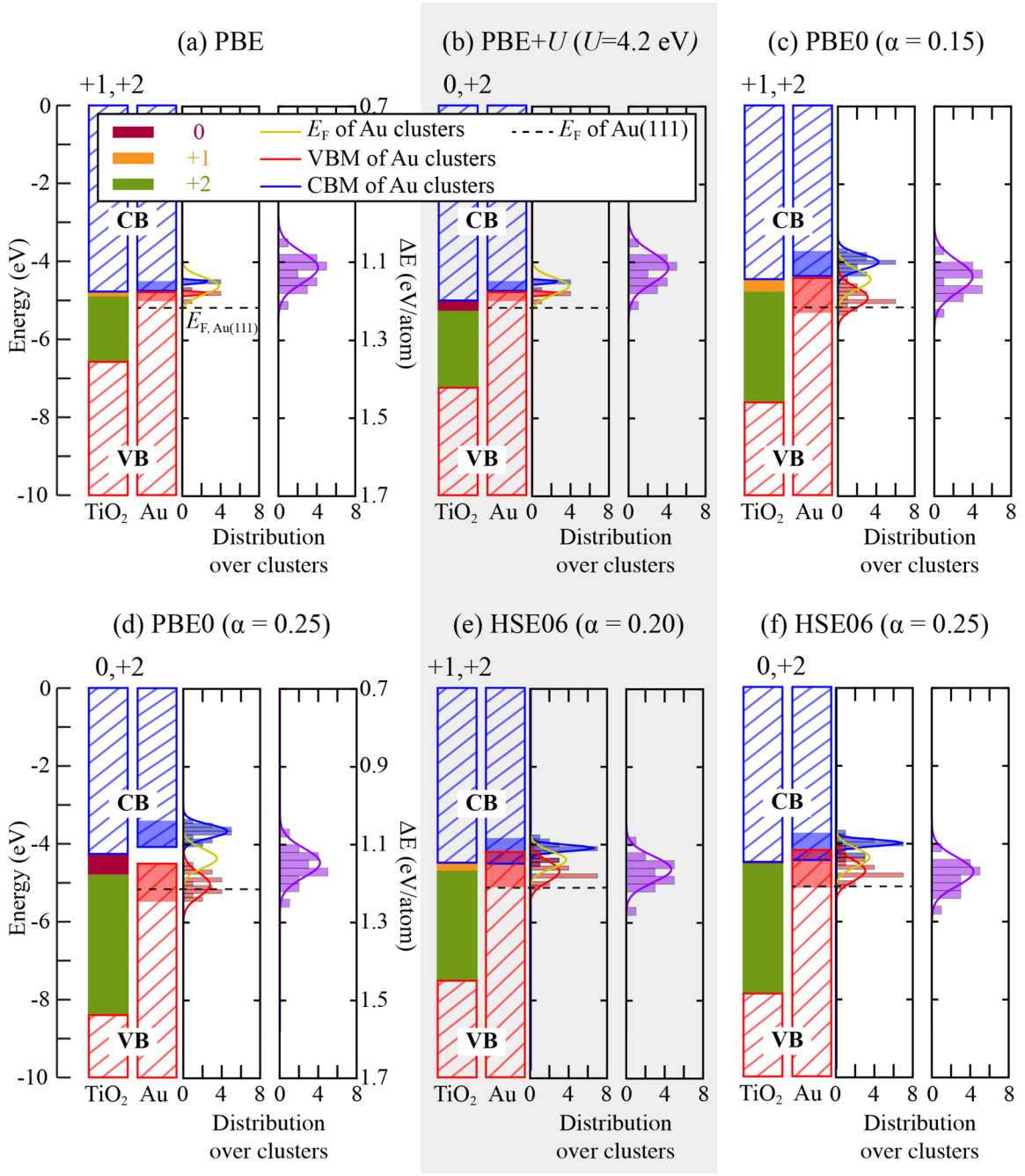

Figure 5. Band alignment in the Au-cluster/V_O:TiO_2 system shown on an absolute scale for all the functionals used within the present study. VB states are shown as red dashed areas, CB states are shown as blue dashed areas. Energy ranges within the TiO_2 band gap associated with different stable V_O charge states are shown as differently colored areas. The respective charge values are listed above the band structure. The spread of VBM and CBM obtained for the gold clusters are shown as red, respectively blue, shaded areas in the Au band structure. The distribution of the values is seen in the connected histogram. The second histogram with purple bars shows for each cluster the average energy of Au atoms in a cluster relative to the energy of a gold atom in Au bulk. The position of the bulk Au Fermi energy E_F is indicated by a dashed black line, aligned via the work function of the Au (111) surface.

From the above discussion we can conclude that the vacancy will not be able to charge (or discharge) the Au clusters. This result is independent of the choice of the xc-functional and can be considered as safe. An ionic binding between a TiO_2 surface vacancy and the Au clusters as has been proposed in some previous studies[16,21] can thus be excluded.

Nature of the Interaction between the Reduced TiO_2 Surface and the Au Cluster. Since the above analysis clearly shows that the commonly assumed picture of an attractive interaction between cluster and vacancy by charge transfer does not hold, we investigate in the following the character of the interaction. For this purpose, we study the response of the electronic charge density when the two separate systems—the isolated Au cluster and the TiO_2 surface with a vacancy—are brought together. We do this by taking first a snapshot of the full system (TiO_2 surface including both the vacancy and Au cluster) and compute its charge density. In a second step, we compute the charge density of the isolated systems (surface

DOI: 10.1021/acs.jpcc.8b12015
J. Phys. Chem. C 2019, 123, 5495−5506

with vacancy and separately the cluster) using the identical supercell and atomic coordinates as for the full system. The resulting integrated total difference charge density is by construction zero and reveals locally in 3D space how the electronic charge rearranges when cluster and surface are brought together.

The resulting difference charge densities are shown in Figure 6 for our three representative cluster configurations. Panel (a)

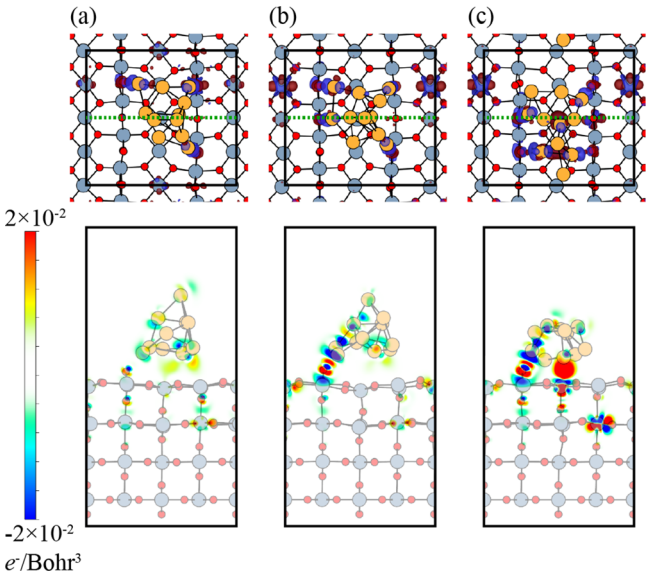

Figure 6. Electron density differences ($\Delta\rho$ = $\rho_{\text{Au-cluster/V}_O\text{:TiO}_2}$ − $\rho_{\text{V}_O\text{:TiO}_2}$ − $\rho_{\text{Au-cluster}}$) showing the redistribution of electron density upon adsorption of the Au cluster on the reduced TiO_2 surface for three Au-cluster/V_O:TiO_2 structures extracted from an AIMD trajectory: (a) the initial structure, (b) the structure with the highest VBM, and (c) the structure with the lowest VBM. The top panels show a top view of the 3D electron density distribution, together with the respective structural arrangement of the atoms. The bottom panels show a 2D cut along the green dashed line seen in the respective top panel, through a plane containing the oxygen vacancy. Red (blue) areas correspond to electron accumulation (depletion). The shown electron difference densities are for an HSE06 calculations with an optimized mixing parameter (α = 0.20). Electron difference density plots obtained from calculations with the other considered exchange-correlation functionals are similar and thus not depicted.

of Figure 6 represents the first snapshot in the AIMD simulation. This configuration is not yet fully equilibrated and shows a comparatively modest electron charge redistribution, as well as the indication of a bond between the surface oxygen vacancy and the gold cluster. The other two configurations sampled from the equilibrated part of the simulation represent two extreme cases with the VBM level of the Au cluster being highest/lowest. In both cases there is no charge transfer between the TiO_2 oxygen vacancy and the gold cluster, in agreement with our conclusions from the alignment analysis. Similarly, the noticeable charge redistribution between the Au cluster with a VBM above the TiO_2 CBM seen in Figure 6b and leading to the formation of an ionic bond, is expected. The equally prominent charge redistribution seen in Figure 6c for a gold cluster with a VBM below the TiO_2 CBM is, in contrast, unexpected and seemingly contradicts the findings of the band diagram analysis. This apparent discrepancy can be resolved by taking into account that the electronic charge densities are not rigid, but will be modified in the contact region where the two densities overlap. To be more specific, in this region hybridization between the orbitals of the two systems will occur and lead to the formation of bonding and antibonding orbitals. These hybridized states may be regarded as polarized covalent bonds.

Keeping this in mind, we can now inspect some of the individual interface features of Figure 6, parts b and c. The most striking difference between them is the strong charge accumulation seen at the Au/TiO_2 interface in Figure 6c, which is absent in Figure 6b. We believe that the ability of the Au cluster in Figure 6b to transfer part of its charge to the CB of TiO_2 localizes the charge redistribution in the regions where the two systems come closest together. In this region of closest proximity the atoms at the edge of the Au cluster approach the bridging O atoms at the TiO_2 surface, which are slightly protruding. As a consequence, a significant part of the charge which would have otherwise participated in bonding via the hybridization mechanism is already bound. This does not happen when the VBM of the Au cluster is located below the CBM of the TiO_2 substrate. If this is the case, all the Au cluster valence electrons are available to form bonds via hybridization. This enables the formation of the highly localized bond seen in the middle of the Au-cluster/TiO_2 interface. This bond is formed in addition to the already existing bonds between the interface Au atoms at the periphery of the cluster and the bridging O atoms protruding from the TiO_2 surface. The observed stronger charge redistribution at the interface in Figure 6c results in a stronger binding between Au cluster and reduced TiO_2 surface, with an ≈0.5 eV stronger binding energy compared to the system in Figure 6b.

The absence of a direct interaction between the TiO_2 surface oxygen vacancy and the Au cluster raises questions about the role of the oxygen vacancy. Two points are particularly puzzling: Why does the cluster remain at the vacancy, as seen in our AIMD simulations and discussed in both the computational and experimental literature,[13,15] and why is the reduced TiO_2 surface/Au cluster catalytically more active than the system without a vacancy? A possible answer to both of these questions is that the absence of a bond between the cluster and the vacancy makes the atoms in its vicinity more polarizable. As a consequence, the Au cluster binds stronger to the TiO_2 substrate. There is a significant charge redistribution at the interface, which makes these sites more reactive. Indeed, our nanocatalyst model studied here in detail has already been instrumental to explain the mechanism of both, methanol oxidation[24,26] and oxygen activation[73] using Au/TiO_2 catalysts in concert with joint experiments. This is in accord with similar studies where interfacial (or "perimeter") sites have been shown to be catalytically highly active.[25,74] Thus, we conclude that the presence of the vacancy indirectly enhances the performance of the nanocatalyst.

CONCLUSIONS AND OUTLOOK

In conclusion, by combining methodologies common to semiconductor physics[46] with ab initio molecular dynamics[45] as used in recent years for dynamical investigations of heterogeneously catalyzed chemical reactions,[75] we are able to elucidate the role of oxygen vacancies in the catalytically active system consisting of a gold nanocluster adsorbed on a reduced TiO_2 (110) surface. The construction of band alignment diagrams enabled us to discuss the amount and direction of electronic charge transfer between the adsorbed

DOI: 10.1021/acs.jpcc.8b12015
J. Phys. Chem. C 2019, 123, 5495−5506

gold cluster and the reduced TiO_2 substrate. Despite the carefully disclosed deficiencies of current exchange-correlation functionals, which cause substantial differences in the constructed band diagrams, we nevertheless consistently find that there is no net charge transfer between the surface oxygen vacancy and the adsorbed Au nanoclusters, which is in stark contrast to the existing and physically highly intuitive picture in favor of such a mechanism. While the commonly expected mechanism is absent, a charge transfer from the Au cluster to the TiO_2 conduction band results in positively charged Au clusters. An in-depth analysis of the electronic structure of the Au/TiO_2 system reveals that the role of the vacancy is indirect in nature. By enhancing the polarizability of the atoms in its vicinity, it induces stronger binding between cluster and substrate. Moreover, this mechanism results in a charge redistribution right at the interface, which increases the reactivity of the supported gold nanoparticle.

The approach devised and implemented in this study is general and can be readily applied to analyze the direction and magnitude of charge transfer of nanocatalysts or clusters deposited or grown on surfaces beyond the specific gold/titania system studied here. Significant steps beyond this status could be to study the activation of dioxygen, O_2, at perimeter sites as used in direct oxidation reactions, or the impact of aqueous solutions on charge transfer and electronic polarization effects in the realm of liquid-phase heterogeneous catalysis. The latter complexity level could be reached by extending our semiconductor physics approach to electrochemistry including the impact of the solvent[76] and electric fields.[77]

AUTHOR INFORMATION

Corresponding Author

*(M.T.) E-mail: m.todorova@mpie.de.

ORCID

Mira Todorova: 0000-0002-8053-9350

Notes

The authors declare no competing financial interest.

ACKNOWLEDGMENTS

This work is supported by the Cluster of Excellence RESOLV (EXC 2033) funded by the Deutsche Forschungsgemeinschaft.

REFERENCES

(1) Haruta, M. Size- and Support-Dependency in the Catalysis of Gold. *Catal. Today* **1997**, *36*, 153.

(2) Meyer, R.; Lemire, C.; Shaikhutdinov, S. K.; Freund, H.-J. Surface Chemistry of Catalysis by Gold. *Gold Bull.* **2004**, *37*, 72.

(3) Roldan Cuenya, B. Metal Nanoparticle Catalysts Beginning to Shape-up. *Acc. Chem. Res.* **2013**, *46*, 1682.

(4) Andreeva, D.; Idakiev, V.; Tabakova, T.; Andreev, A. Low-Temperature Water-Gas Shift Reaction over Au/α-Fe_2O_3. *J. Catal.* **1996**, *158*, 354.

(5) Fu, Q.; Saltsburg, H.; Flytzani-Stephanopoulos, M. Active Nonmetallic Au and Pt Species on Ceria-Based Water-Gas Shift Catalysts. *Science* **2003**, *301*, 935.

(6) Haruta, M.; Kobayashi, T.; Sano, H.; Yamada, N. Novel Gold Catalysts for the Oxidation of Carbon Monoxide at a Temperature far Below 0°C. *Chem. Lett.* **1987**, *16*, 405.

(7) Bond, G. C.; Thompson, D. T. Gold-Catalysed Oxidation of Carbon Monoxide. *Gold Bull.* **2000**, *33*, 41.

(8) Kung, M. C.; Davis, R. J.; Kung, H. H. Understanding Au-Catalyzed Low-Temperature CO Oxidation. *J. Phys. Chem. C* **2007**, *111*, 11767.

(9) Widmann, D.; Krautsieder, A.; Walter, P.; Brückner, A.; Behm, R. J. How Temperature Affects the Mechanism of CO Oxidation on Au/TiO_2: A Combined EPR and TAP Reactor Study of the Reactive Removal of TiO_2 Surface Lattice Oxygen in Au/TiO_2 by CO. *ACS Catal.* **2016**, *6*, 5005.

(10) Wang, Y.; Widmann, D.; Behm, R. J. Inuence of TiO_2 Bulk Defects on CO Adsorption and CO Oxidation on Au/TiO_2: Electronic Metal-Support Interactions (EMSIs) in Supported Au Catalysts. *ACS Catal.* **2017**, *7*, 2339.

(11) Lopez, N.; Nørskov, J. K.; Janssens, T. V. W.; Carlsson, A.; Puig-Molina, A.; Clausens, B.; Grunwaldt, J.-D. The Adhesion and Shape of Nanosized Au Particles in a Au/TiO_2 Catalyst. *J. Catal.* **2004**, *225*, 86.

(12) Molina, L. M.; Rasmussen, M. D.; Hammer, B. Adsorption of O_2 and Oxidation of CO at Au Nanoparticles Supported by $TiO_2(110)$. *J. Chem. Phys.* **2004**, *120*, 7673.

(13) Wahlström, E.; Lopez, N.; Schaub, R.; Thostrup, P.; Rønnau, A.; Africh, C.; Lægsgaard, E.; Nørskov, J. K.; Besenbacher, F. Bonding of Gold Nanoclusters to Oxygen Vacancies on Rutile $TiO_2(110)$. *Phys. Rev. Lett.* **2003**, *90*, 026101.

(14) Wörz, A. S.; Heiz, U.; Cinquini, F.; Pacchioni, G. Charging of Au Atoms on TiO_2 Thin Films from CO Vibrational Spectroscopy and DFT Calculations. *J. Phys. Chem. B* **2005**, *109*, 18418.

(15) Dong, W.; Reichenberger, S.; Chu, S.; Weide, P.; Ruland, H.; Barcikowski, S.; Wagener, P.; Muhler, M. The Effect of the Au Loading on the Liquid-Phase Aerobic Oxidation of Ethanol over Au/TiO_2 Catalysts Prepared by Pulsed Laser Ablation. *J. Catal.* **2015**, *330*, 497.

(16) Wang, Y.; Hwang, G. S. Adsorption of Au Atoms on Stoichiometric and Reduced $TiO_2(110)$ Rutile Surfaces: a First Principles Study. *Surf. Sci.* **2003**, *542*, 72.

(17) Iddir, H.; Öğüt, S.; Browning, N. D.; Disko, M. M. Adsorption and Diffusion of Pt and Au on the Stoichiometric and Reduced TiO_2 Rutile (110) Surfaces. *Phys. Rev. B* **2005**, *72*, 081407.

(18) Farnesi Camellone, M.; Kowalski, P. M.; Marx, D. Ideal, Defective, and Gold-Promoted Rutile $TiO_2(110)$ Surfaces Interacting with CO, H_2, and H_2O: Structures, Energies, Thermodynamics, and Dynamics from PBE+U. *Phys. Rev. B* **2011**, *84*, 035413.

(19) Farnesi Camellone, M.; Marx, D. On the Impact of Solvation on a Au/TiO_2 Nanocatalyst in Contact with Water. *J. Phys. Chem. Lett.* **2013**, *4*, 514.

(20) Pabisiak, T.; Kiejna, A. First-Principles Study of Au Nanostructures on Rutile $TiO_2(110)$. *Phys. Rev. B* **2009**, *79*, 085411.

(21) Hong, S.; Rahman, T. S. Rationale of the Higher Reactivity of Interfacial Sites in Methanol Decomposition on $Au13/TiO_2(110)$. *J. Am. Chem. Soc.* **2013**, *135*, 7629.

(22) Okazaki, K.; Morikawa, Y.; Tanaka, S.; Tanaka, K.; Kohyama, M. Electronic Structures of Au on $TiO_2(110)$ by First-Principles Calculations. *Phys. Rev. B* **2004**, *69*, 235404.

(23) Chrétien, S.; Metiu, H. Density Functionals Study of the Interaction between Small Au Clusters, Au_n (n = 1−7) and the Rutile TiO_2 Surface. II. Adsorption on a Partially Reduced Surface. *J. Chem. Phys.* **2007**, *127*, 244708.

(24) Farnesi Camellone, M.; Zhao, J.; Jin, L.; Wang, Y.; Muhler, M.; Marx, D. Molecular Understanding of Reactivity and Selectivity for Methanol Oxidation at the Au/TiO_2 Interface. *Angew. Chem., Int. Ed.* **2013**, *52*, 5780.

(25) Wang, Y.-G.; Yoon, Y.; Glezakou, V.-A.; Li, J.; Rousseau, R. The Role of Reducible Oxide-Metal Cluster Charge Transfer in Catalytic Processes: New Insights on the Catalytic Mechanism of CO Oxidation on Au/TiO_2 from Ab Initio Molecular Dynamics. *J. Am. Chem. Soc.* **2013**, *135*, 10673.

(26) Farnesi Camellone, M.; Marx, D. Nature and Role of Activated Molecular Oxygen Species at the Gold/Titania Interface in the Selective Oxidation of Alcohols. *J. Phys. Chem. C* **2014**, *118*, 20989.

(27) Wang, Y.-G.; Cantu, D. C.; Lee, M.-S.; Li, J.; Glezakou, V.-A.; Rousseau, R. CO Oxidation on Au/TiO_2: Condition-Dependent Active Sites and Mechanistic Pathways. *J. Am. Chem. Soc.* **2016**, *138*, 10467.

DOI: 10.1021/acs.jpcc.8b12015
J. Phys. Chem. C 2019, 123, 5495−5506

(28) Muñoz-Santiburcio, D.; Farnesi Camellone, M.; Marx, D. Solvation-Induced Changes in the Mechanism of Alcohol Oxidation at Gold/Titania Nanocatalysts in the Aqueous Phase versus Gas Phase. *Angew. Chem., Int. Ed.* **2018**, *57*, 3327.
(29) Haruta, M.; Tsubota, S.; Kobayashi, T.; Kageyama, H.; Genet, M. J.; Delmon, B. Low-Temperature Oxidation of CO over Gold Supported on TiO_2 α-Fe_2O_3, and Co_3O_4. *J. Catal.* **1993**, *144*, 175.
(30) Liu, H.; Kozlov, A. I.; Kozlova, A. P.; Shido, T.; Asakura, K.; Iwasawa, Y. Active Oxygen Species and Mechanism for Low-Temperature CO Oxidation Reaction on a TiO_2-Supported Au Catalyst Prepared from $Au(PPh_3)(NO_3)$ and As-Precipitated Titanium Hydroxide. *J. Catal.* **1999**, *185*, 252.
(31) Bamwenda, G. R.; Tsubota, S.; Nakamura, T.; Haruta, M. The Inuence of the Preparation Methods on the Catalytic Activity of Platinum and Gold Supported on TiO_2 for CO Oxidation. *Catal. Lett.* **1997**, *44*, 83.
(32) Henao, J. D.; Caputo, T.; Yang, J. H.; Kung, M. C.; Kung, H. H. In Situ Transient FTIR and XANES Studies of the Evolution of Surface Species in CO Oxidation on Au/TiO_2. *J. Phys. Chem. B* **2006**, *110*, 8689.
(33) Overbury, S. H.; Schwartz, V.; Mullins, D. R.; Yan, W.; Dai, S. Evaluation of the Au Size Effect: CO Oxidation Catalyzed by Au/TiO_2. *J. Catal.* **2006**, *241*, 56.
(34) Janssens, T. V. W.; Carlsson, A.; Puig-Molina, A.; Clausen, B. S. Relation between Nanoscale Au Particle Structure and Activity for CO Oxidation on Supported Gold Catalysts. *J. Catal.* **2006**, *240*, 108.
(35) Comotti, M.; Li, W.-C.; Spliethoff, B.; Schüth, F. Support Effect in High Activity Gold Catalysts for CO Oxidation. *J. Am. Chem. Soc.* **2006**, *128*, 917.
(36) Weiher, N.; Beesley, A. M.; Tsapatsaris, N.; Delannoy, L.; Louis, C.; van Bokhoven, J. A.; Schroeder, S. L. M. Activation of Oxygen by Metallic Gold in Au/TiO_2 Catalysts. *J. Am. Chem. Soc.* **2007**, *129*, 2240.
(37) Arrii, S.; Morfin, F.; Renouprez, A. J.; Rousset, J. L. Oxidation of CO on Gold Supported Catalysts Prepared by Laser Vaporization: Direct Evidence of Support Contribution. *J. Am. Chem. Soc.* **2004**, *126*, 1199.
(38) Widmann, D.; Behm, R. J. Activation of Molecular Oxygen and the Nature of the Active Oxygen Species for CO Oxidation on Oxide Supported Au Catalysts. *Acc. Chem. Res.* **2014**, *47*, 740.
(39) Ceperley, D. M.; Alder, B. J. Ground State of the Electron Gas by a Stochastic Method. *Phys. Rev. Lett.* **1980**, *45*, 566.
(40) Perdew, J. P.; Burke, K.; Ernzerhof, M. Generalized Gradient Approximation Made Simple. *Phys. Rev. Lett.* **1996**, *77*, 3865.
(41) Perdew, J. P.; Ernzerhof, M.; Burke, K. Rationale for Mixing Exact Exchange With Density Functional Approximations. *J. Chem. Phys.* **1996**, *105*, 9982.
(42) Adamo, C.; Barone, V. Toward Reliable Density Functional Methods without Adjustable Parameters: The PBE0Model. *J. Chem. Phys.* **1999**, *110*, 6158.
(43) Heyd, J.; Scuseria, G. E.; Ernzerhof, M. Hybrid Functionals Based on a Screened Coulomb Potential. *J. Chem. Phys.* **2003**, *118*, 8207.
(44) Heyd, J.; Scuseria, G. E.; Ernzerhof, M. Erratum: Hybrid Functionals Based on a Screened Coulomb Potential [J. Chem. Phys. 118, 8207 2003]. *J. Chem. Phys.* **2006**, *124*, 219906.
(45) Marx, D.; Hutter, J. *Ab Initio Molecular Dynamics: Basic Theory and Advanced Methods*; Cambridge University Press: 2009.
(46) Freysoldt, C.; Grabowski, B.; Hickel, T.; Neugebauer, J.; Kresse, G.; Janotti, A.; Van de Walle, C. G. First-Principles Calculations for Point Defects in Solids. *Rev. Mod. Phys.* **2014**, *86*, 253.
(47) Janotti, A.; Varley, J. B.; Rinke, P.; Umezawa, N.; Kresse, G.; Van de Walle, C. G. Hybrid Functional Studies of the Oxygen Vacancy in TiO_2. *Phys. Rev. B* **2010**, *81*, 085212.
(48) Grant, F. A. Properties of Rutile (Titanium Dioxide). *Rev. Mod. Phys.* **1959**, *31*, 646.
(49) Lide, D. R., Ed. *CRC Handbook of Chemistry and Physics*; CRC Press: Boca Raton, FL, 2017.
(50) Pascual, J.; Camassel, J.; Mathieu, H. Resolved Quadrupolar Transition in TiO_2. *Phys. Rev. Lett.* **1977**, *39*, 1490.
(51) Pascual, J.; Camassel, J.; Mathieu, H. Fine Structure in the Intrinsic Absorption Edge of TiO_2. *Phys. Rev. B* **1978**, *18*, 5606.
(52) Hölzl, J.; Schulte, F. K. *Work Functions of Metals*; Springer-Verlag Berlin Heidelberg GmbH: 1979; Vol. *85*.
(53) Van de Walle, C. G.; Neugebauer, J. First-Principles Calculations for Defects and Impurities: Applications to III-Nitrides. *J. Appl. Phys.* **2004**, *95*, 3851.
(54) Freysoldt, C.; Neugebauer, J. First-Principles Calculations for Charged Defects at Surfaces, Interfaces, and Two-Dimensional Materials in the Presence of Electric Fields. *Phys. Rev. B* **2018**, *97*, 205425.
(55) Kresse, G.; Hafner, J. Ab Initio Molecular Dynamics for Liquid Metals. *Phys. Rev. B* **1993**, *47*, 558.
(56) Kresse, G.; Hafner, J. Ab Initio Molecular-Dynamics Simulation of the Liquid-Metal Amorphous-Semiconductor Transition in Germanium. *Phys. Rev. B* **1994**, *49*, 14251.
(57) Kresse, G.; Furthmüller, J. Efficient Iterative Schemes for Ab Initio Total-Energy Calculations Using a Plane-Wave Basis Set. *Phys. Rev. B* **1996**, *54*, 11169.
(58) Kresse, G.; Furthmüller, J. Efficiency of Ab-Initio Total Energy Calculations for Metals and Semiconductors Using a Plane-Wave Basis Set. *Comput. Mater. Sci.* **1996**, *6*, 15.
(59) Kresse, G.; Joubert, D. From Ultrasoft Pseudopotentials to the Projector Augmented-Wave Method. *Phys. Rev. B* **1999**, *59*, 1758.
(60) Blöchl, P. E. Projector Augmented-Wave Method. *Phys. Rev. B* **1994**, *50*, 17953.
(61) Perdew, J. P.; Burke, K.; Ernzerhof, M. Generalized Gradient Approximation Made Simple [Phys. Rev. Lett. 77, 3865 (1996)]. *Phys. Rev. Lett.* **1997**, *78*, 1396.
(62) Cococcioni, M.; de Gironcoli, S. Linear Response Approach to the Calculation of the Effective Interaction Parameters in the LDA+U Method. *Phys. Rev. B* **2005**, *71*, 035105.
(63) Nair, N. N.; Ribas-Arino, J.; Staemmler, V.; Marx, D. Magnetostructural Dynamics from Hubbard-U Corrected Spin-Projection: [2Fe-2S] Complex in Ferredoxin. *J. Chem. Theory Comput.* **2010**, *6*, 569.
(64) Kowalski, P. M.; Camellone, M.; Nair, N. N.; Meyer, B.; Marx, D. Charge Localization Dynamics Induced by Oxygen Vacancies on the TiO_2(110)Surface. *Phys. Rev. Lett.* **2010**, *105*, 146405.
(65) Dudarev, S. L.; Botton, G. A.; Savrasov, S. Y.; Humphreys, C. J.; Sutton, A. P. Electron-Energy-Loss Spectra and the Structural Stability of Nickel Oxide: An LSDA+U Study. *Phys. Rev. B* **1998**, *57*, 1505.
(66) Krukau, A. V.; Vydrov, O. A.; Izmaylov, A. F.; Scuseria, G. E. Inuence of the Exchange Screening Parameter on the Performance of Screened Hybrid Functionals. *J. Chem. Phys.* **2006**, *125*, 224106.
(67) Kowalski, P. M.; Meyer, B.; Marx, D. Composition, Structure, and Stability of the Rutile TiO_2(110) Surface: Oxygen Depletion, Hydroxylation, Hydrogen Migration, and Water Adsorption. *Phys. Rev. B* **2009**, *79*, 115410.
(68) Brandão, F. D.; Pinheiro, M. V. B.; Ribeiro, G. M.; Medeiros-Ribeiro, G.; Krambrock, K. Identification of Two Light-Induced Charge States of the Oxygen Vacancy in Single-Crystalline Rutile TiO_2. *Phys. Rev. B* **2009**, *80*, 235204.
(69) Brant, A. T.; Golden, E. M.; Giles, N. C.; Yang, S.; Sarker, M. A. R.; Watauchi, S.; Nagao, M.; Tanaka, I.; Tryk, D. A.; Manivannan, A.; et al. Triplet Ground State of the Neutral Oxygen-Vacancy Donor in Rutile TiO_2. *Phys. Rev. B* **2014**, *89*, 115206.
(70) Sarkar, T.; Gopinadhan, K.; Zhou, J.; Saha, S.; Coey, J. M. D.; Feng, Y. P.; Ariando; Venkatesan, T. Electron Transport at the TiO_2 Surfaces of Rutile, Anatase, and Strontium Titanate: The Inuence of Orbital Corrugation. *ACS Appl. Mater. Interfaces* **2015**, *7*, 24616.
(71) Queisser, H. J.; Haller, E. E. Defects in Semiconductors: Some Fatal, Some Vital. *Science* **1998**, *281*, 945.
(72) Hutter, J., et al., CPMD Program Package. http://www.cpmd.org.
(73) Siemer, N.; Lüken, A.; Zalibera, M.; Frenzel, J.; Muñoz-Santiburcio, D.; Savitsky, A.; Lubitz, W.; Muhler, M.; Marx, D.;

DOI: 10.1021/acs.jpcc.8b12015
J. Phys. Chem. C 2019, 123, 5495−5506

Strunk, J. Atomic Scale Explanation of O_2 Activation at the Au-TiO_2 Interface. *J. Am. Chem. Soc.* **2018**, *140*, 18082.
(74) Green, I. X.; Tang, W.; Neurock, M.; Yates, J. T. Spectroscopic Observation of Dual Catalytic Sites During Oxidation of CO on a Au/TiO_2 Catalyst. *Science* **2011**, *333*, 736.
(75) Frenzel, J.; Kiss, J.; Nair, N. N.; Meyer, B.; Marx, D. Methanol Synthesis on ZnO from Molecular Dynamics. *Phys. Status Solidi B* **2013**, *250*, 1174.
(76) Yoo, S.-H.; Todorova, M.; Neugebauer, J. Selective Solvent-Induced Stabilization of Polar Oxide Surfaces in an Electrochemical Environment. *Phys. Rev. Lett.* **2018**, *120*, 066101.
(77) Surendralal, S.; Todorova, M.; Finnis, M. W.; Neugebauer, J. First-Principles Approach to Model Electrochemical Reactions: Understanding the Fundamental Mechanisms Behind Mg Corrosion. *Phys. Rev. Lett.* **2018**, *120*, 246801.

DOI: 10.1021/acs.jpcc.8b12015
J. Phys. Chem. C 2019, 123, 5495−5506